Applied Catalysis B: Environmental 148–149 (2014) 221–230

Contents lists available at ScienceDirect

Applied Catalysis B: Environmental

journal homepage: www.elsevier.com/locate/apcatb

Effect of the divalent metal and the activation temperature of NiMoW and CoMoW on the dibenzothiophene hydrodesulfurization reaction

Sandra L. Amaya[a], G. Alonso-Núñez[b], T.A. Zepeda[b], S. Fuentes[b], Adriana Echavarría[a,*]

[a] Grupo Catalizadores y Adsorbentes, Universidad de Antioquia-UdeA, A.A 1226 - Medellín, Colombia
[b] Universidad Nacional Autónoma de México, Centro de Nanociencias y Nanotecnología, Ensenada, Baja California, C.P. 22860, Mexico

ARTICLE INFO

Article history:
Received 10 May 2013
Received in revised form 28 October 2013
Accepted 29 October 2013
Available online 7 November 2013

Keywords:
Dibenzothiophene
Hydrodesulfurization
Activation
Unsupported catalyst

ABSTRACT

α and β trimetallic mixed oxides were obtained from ϕ_y layered phase precursors with $(NH_4)H_{1.4}Ni_{2.3}O(OH)(MoO_4)_{1.4}(WO_4)_{0.6}$ and $(NH_4)H_2Co_2O(OH)(MoO_4)_{1.6}(WO_4)_{0.4}$ formulas by calcination at temperatures as low as 673 K. At this temperature, phase transition was confirmed by (TGA and DSC) thermal analysis. Oxides were activated *ex-situ* under a H_2S/H_2 (15%, v/v) mixture at two temperatures: 673 K and 798 K, to obtain metal sulfides phases, which were active catalysts in the hydrodesulfurization reaction of dibenzothiophene. The effect of the (Ni, Co) promoter and the activation temperature were studied to know the behavior and adequate activation conditions. X-ray photoelectron spectroscopy (XPS) and hydrogen temperature-programmed reduction (H_2-TPR) provided useful information about the oxidation states of the metallic species in the mixed oxides, which were related to the catalytic activity in the hydrotreating reaction. Sulfided catalysts were also characterized by scanning electron microscopy (SEM) and transmission electron microscopy (TEM) for understanding their textural and morphological differences. Additional characterization was carried out using BET surface area and elemental analysis. All catalysts were tested in the hydrodesulfurization (HDS) of dibenzothiophene (DBT) at 593 K and 5.5 MPa. The best catalytic behavior was obtained using Ni as promoter, activated at 798 K. Nickel catalysts were more hydrogenating than cobalt catalysts.

1. Introduction

Nowadays, new deposits of crude oils have been found, but they contain high amount of sulfur and nitrogen making the process for fuels production difficult. The negative impact in the environment [1,2], along with problems in the processing units [1], has encouraged the refining industry to find solutions. Currently, there are numerous researches related to variations in the process conditions, modification of existing catalysts [1–5] or preparation of new catalysts [2,3]; these efforts are being oriented to reduce the high content of S, N, O heteroatoms in the feeds.

Preparation of new active catalysts in the HDS reaction has been subject of great interest for the industry and scientific communities since 40–50 years ago [6]. Hydrotreating catalysts commonly comprise molybdenum or tungsten sulfide, promoted with nickel or cobalt and supported on alumina [7]. Some reports with unsupported sulfides have appeared in the open literature, the most commonly being NiMo sulfides; but other combinations with Co and W have also been tested [8–10]; almost all these catalysts were synthesized using thio-salt precursors to incorporate the sulfur. Another way to prepare unsupported catalysts for HDT is through metal oxide precursors, which are subsequently activated with sulfur compounds; however, this route present a disadvantage due to the low surface of mixed oxides [11]. To overcome this, layered precursors could be used to obtain the mixed oxides with high surface areas. This type of materials generally produces volatile compounds during calcination, which may generate porosity and therefore high surface areas. Furthermore, since a bimetallic precursor compound is obtained, mixing of the metals occurs at a molecular level and therefore good mixing of the active metals is expected after calcination and subsequent sulfidation.

Layered phases have been studied by several researchers [12–14]; their oxides have been evaluated in different reactions such as oxidation of propene, hydrogenation of naphthalene, *etc.* [15]. The ϕ_y phase, composed by Ni and Mo, is a layered material which was reported by Levin et al. [12]. This phase corresponds to the ideal formula $(NH_4)Ni_2Mo_2O_8(OH)\cdot H_2O$, and its structure consists of endless chains of NiO_6 octahedra connected through MoO_4 tetrahedra, sharing two vertices with consecutive elements in one chain, extending the third vertex to an adjacent chain; the fourth vertex protrudes into the interlayer space. Among the layers, the ammonium ions compensate the net negative charge of the layers.

In this research, trimetallic mixed oxides with high surface area were prepared [11,16–19] by calcination of ϕ_y layer precursors.

* Corresponding author.
E-mail address: adriana.echavarria@udea.edu.co (A. Echavarría).

0926-3373/$ – see front matter © 2013 Elsevier B.V. All rights reserved.
http://dx.doi.org/10.1016/j.apcatb.2013.10.057

Then, the mixed oxides were activated by heating *ex-situ* under a H_2S/H_2 (15%, v/v) mixture, before testing them in DBT hydrodesulfurization reactions. The purpose of this work was to understand how the nickel and cobalt as promoters are affected by the activation temperature on the DBT hydrodesulfurization reaction. All the sulfided catalysts were characterized by XRD, N_2-physisorption, SEM and TEM.

2. Experimental

2.1. Reactants

Layered precursors containing Ni-Mo-W and Co-Mo-W were prepared using $NiSO_4{\cdot}6H_2O$ (Merck, 99%), $Co(NO_3)_2{\cdot}6H_2O$ (Vetec, 98%), $(NH_4)_6Mo_7O_{24}{\cdot}4H_2O$ (Merck, 99%), $(NH_4)_{10}W_{12}O_{39}{\cdot}5H_2O$ (Alfa Aesar), and NH_4OH solution (J.T Baker, 28–30%).

2.2. Preparation of the catalysts

The syntheses of the layered precursors were based on reported methods [12,13], but some modifications were carried out. Briefly, the precursors were synthesized by co-precipitation (CoMoW) and hydrothermal (NiMoW) methods. Solutions containing the metal salts were separately prepared and then mixed, always adding the nickel (or cobalt) solution to the other ones; ammonia was used as a precipitating agent. In the co-precipitation method, the slurry produced was maintained at 298 K under stirring during 4 h. In the hydrothermal method, additionally, the mixture was heated at 473 K for 96 h in Teflon-lined autoclaves. After the heating, the solids were filtered, washed with water, and dried at 373 K. The molar compositions in both precursors with respect to 1 mol of $NiSO_4$ and $Co(NO_3)_2$ were $NiSO_4$:0.11$(NH_4)_6Mo_7O_{24}$:0.02$(NH_4)_{10}W_{12}O_{39}$:2.90NH_4OH:188 H_2O, and $Co(NO_3)_2$:0.11$(NH_4)_6Mo_7O_{24}$:0.02$(NH_4)_{10}W_{12}O_{39}$:1.43 NH_4OH:264 H_2O, to obtain the corresponding trimetallic layered precursors: $(NH_4)H_{1.4}Ni_{2.3}O(OH)(MoO_4)_{1.4}(WO_4)_{0.6}$ and $(NH_4)H_2Co_2O(OH)(MoO_4)_{1.6}(WO_4)_{0.4}$ called as Ni-L and Co-L, respectively.

Then, the layered precursors were calcined at 673 K for 3 h at a rate of 5 K/min, in order to obtain the porous mixed oxides (Ni-O and Co-O) with high surface area. The precursors and mixed oxides were labeled as is shown in Table 1.

2.3. Activation of the mixed oxides

Ni-O and Co-O were sulfided by heating *ex-situ* under a H_2S/H_2 (15%, v/v) mixture from 298 K to 673 or 798 K for 4 h with a heating rate of 5 K/min. The obtained catalysts were kept under argon atmosphere to prevent oxidation during transfer to the batch reactor. The catalysts were labeled according to Table 1, indicating the promoter (Ni or Co), the state of trimetallic material (O: oxide, S: sulfide and SR: sulfided after reaction), and the activation temperature.

2.4. Characterization of catalysts

2.4.1. Elemental analysis

The metal content analysis for layered precursors was carried out in a Thermo Scientific ICE Series 3000 equipment. All samples were treated with mineral acids (hydrochloric, nitric and phosphoric acids) to achieve a complete dissolution. Interferences associated with each metal were corrected with the nitrous oxide and acetylene flame. Analyses were performed in duplicate.

2.4.2. BET surface area

The surface areas of the mixed oxides were measured in a Micromeritics ASAP 2010 equipment by nitrogen adsorption at 77 K, using the BET method, from isotherms measured by the volumetric method. Materials were degassed at temperatures between 523 and 573 K. The surface areas of the sulfided samples were measured in a Micromeritics Tristar II by nitrogen adsorption at 77 K, using the BET method, from isotherms measured by the volumetric method. The sample weight was of 0.2–0.3 g. Samples were degassed in a Micromeritics VacPrep 061 at 473 K for 5 h before nitrogen adsorption. The pore size distribution and total pore volume were obtained from the desorption data following the BJH method.

2.4.3. X-ray diffraction

Mixed oxides were characterized by XRD in a Rigaku Miniflex diffractometer with CuK_α radiation, at $\lambda = 0.15418$ nm, 40 kV and 30 mA. Samples were analyzed in a range of 3–40° (2θ) at 2°/min. Layered precursors and sulfided materials were characterized by XRD in a Philips X Pert diffractometer at room temperature with a CuK_α radiation, at $\lambda = 0.15406$ nm, 45 kV and 40 mA. Samples were analyzed in a range of 10–80° (2θ) with a step size of 0.02°. The sulfided samples were treated with an argon flow to avoid the oxidation.

2.4.4. TGA and DSC analysis

Thermogravimetric analysis of the layered precursors was carried-out in a TA Instruments Hi-Res 2950 apparatus, with a heating rate of 10 K/min, in the 298–1073 K range under a 40 ml/min nitrogen flow. Differential scanning calorimetry was performed in a TA-Instruments 2920 equipment with a heating rate of 5 K/min under nitrogen atmosphere.

2.4.5. H_2-TPR measurements

H_2-TPR measurements of the mixed oxides were carried-out in a Zeton Altamira AMI-90 equipment. Initially, a pre-treatment was performed by heating from room temperature to 573 K, in an argon atmosphere. Then, the reduction of the mixed oxides was carried-out with a flow of 30 ml/min of a mixture of 10 vol% H_2 in Ar, and increasing the temperature from room-temperature to 1273 K at a rate of 10 K/min.

2.4.6. X-ray photoelectron spectroscopy (XPS)

XPS spectra of the mixed oxides were recorded using a Leybold LHS-18 spectrometer equipped with an AlK_α monochromatic source (1486.6 eV) and an EA-10 semi-spherical analyzer. Binding energy is related to the adventitious C1s line at 284.6 eV. Collected spectra were analyzed using SPECTRA presenter and XPS Peak 4.1.

2.4.7. Scanning electron microscopy (SEM)

Scanning electron micrographs and energy-dispersive X-ray spectroscopy (EDS) elemental analysis of the after-reaction materials were obtained using a JEOL 5300 microscope.

2.4.8. Transmission electron microscopy (TEM)

TEM analysis was performed using a JEOL JEM-2010 microscope operating at 200 kV. The after-reaction catalysts were ultrasonically dispersed in isopropanol at room temperature and then the suspensions were collected on a carbon-coated copper grid in order to be analyzed in the microscope.

2.5. Catalytic activity

DBT (Aldrich Chemical, 98%) hydrodesulfurization reactions were carried-out in a Parr model 4848 high-pressure batch reactor. A mixture of 0.23 g DBT and 100 ml hexadecane as solvent (Aldrich Chemical, 99%) was added to the reactor along with 0.22–0.23 g of the sulfided catalyst. The reactor was purged with nitrogen and heated to reach the reaction temperature of 593 K; then it was

Table 1
List of materials and their designations.

	Layer material	Mixed oxide	Sulfidation at 673 and 798 K	Sulfides after reaction
NiMoW	Ni-L	Ni-O	Ni-S673, Ni-S798	Ni-SR673, Ni-SR798
CoMoW	Co-L	Co-O	Co-S673, Co-S798	Co-SR673, Co-SR798

pressurized with hydrogen up to 5.5 MPa, and a stirring rate of 700 rpm was performed. The reaction was monitored during 5 h by chromatographic analysis with an Agilent Technologies 7890A gas chromatograph (GC) using a HP-5 Agilent Alumina capillary column (30 m × 0.32 mm × 0.25 μm).

The compounds detected by GC were biphenyl (BP) through the direct desulfurization (DDS) route and cyclohexylbenzene (CHB) and tetrahydrodibenzothiophene (THDBT) through the hydrogenation (HYD) route. The total DBT conversion (X_{DBT}) was calculated according to Eq. (1); and DDS and HYD selectivity was calculated according to Eqs. (2) and (3), respectively.

$$X_{DBT} = \frac{(CHB + BP + THDBT) \times 100\%}{(DBT + CHB + BP + THDBT)} \quad (1)$$

$$DDS = \frac{BP \times 100\%}{(CHB + BP + THDBT)} \quad (2)$$

$$HYD = \frac{(CHB + THDBT) \times 100\%}{(CHB + BP + THDBT)} \quad (3)$$

The catalytic activity was also expressed in terms of the initial reaction rate (mol DBT transformed per second and per gram of catalyst).

3. Results and discussion

3.1. X-ray diffraction

The X-ray diffractograms of the phase identified in the PDF-4 database and the Ni-L and Co-L precursors obtained in this work are presented in Fig. 1. Materials showed typical reflections of ϕ_y layered phase reported by Levin et al. [12], with a composition of $(NH_4)Ni_2Mo_2O_8(OH)\cdot H_2O$ and identified in the PDF-4 database [20] under number 050-1414, as presented in Fig. 1a. The Ni-L trimetallic material (Fig. 1b) exhibited less crystallinity than Co-L (Fig. 1c). The patterns of both precursors showed small differences in the 2θ peak positions with respect to the materials reported by Levin et al. [12]. This is attributed to the trimetallic character of materials obtained in this research that can lead to differences in the cell dimensions. Evidences of crystalline impurities were not found in Co-L material; however, Ni-L material exhibited signals around 22°, 28°, 36°, 54° and 59° (2θ) that do not correspond to ϕ_y type, and could correspond to an impurity phase. The crystal sizes calculated using the Scherrer equation [21] from the reflection at 26.6° (2θ) were 15.6 nm and 21.3 nm, for Ni-L and Co-L, respectively.

Fig. 2 shows the XRD patterns of the trimetallic mixed oxides, Ni-O (2a) and Co-O (2b) obtained after the calcination treatment of the layered (Ni-L and Co-L) precursors at 673 K. The Co-O material showed peaks characteristic of the β phase described by Mazzocchia et al. [16], and found in the Powder Diffraction File (PDF-4) database under number 021-0868 [20]. On the other hand, the Ni-O material presented peaks attributed to α (033-09-48, PDF-4) phase [18]. α and β-isomorphs, mixed oxides reported by several authors [22–24] with bimetallic systems such as Fe-Mo, Co-Mo and Ni-Mo have been employed as precursors of HDS catalysts. The main difference between α and β-isomorphs is the coordination of hexavalent metal, octahedral in α phase and tetrahedral in β phase. In both cases the divalent metal occupies sites with octahedral coordination [23]. In this work, two trimetallic mixed oxides with composition NiMoW and CoMoW were obtained at 673 K, a temperature below other previously reported temperatures obtained with other systems based on bimetallic systems [22].

The decomposition reactions during the calcination to 673 K of Ni-L and Co-L to obtain Ni-O and Co-O respectively can be expressed by the following chemical equations (4) and (5):

$$(NH_4)H_{1.4}Ni_{2.3}O(OH)(MoO_4)_{1.4}(WO_4)_{0.6} \rightarrow 1.4NiMoO_4 + 0.6NiWO_4 + 0.3NiO + NH_3 + 1.7H_2O \quad (4)$$

$$(NH_4)H_2Co_2O(OH)(MoO_4)_{1.6}(WO_4)_{0.4} \rightarrow 1.6CoMoO_4 + 0.4CoWO_4 + NH_3 + 2H_2O \quad (5)$$

According to Eqs. (4) and (5), two mixed oxides with molybdenum and tungsten were formed; it was confirmed by atomic absorption analyses of the corresponding metals. Based on the XRD results, characteristic signals of tungsten oxides as wolframite phase was not evidenced; therefore, a successful incorporation of tungsten in the observed phase can be suggested.

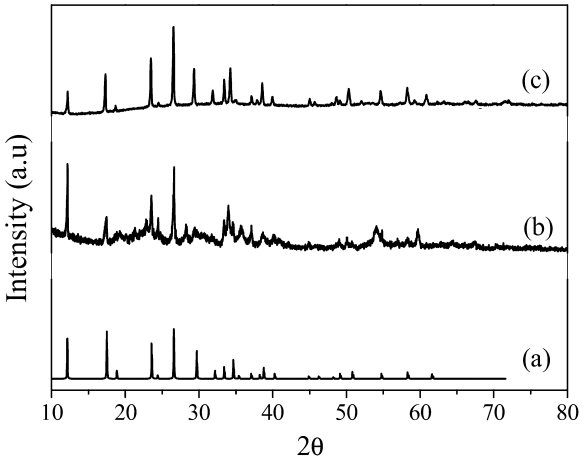

Fig. 1. XRD patterns of precursors (a) NiMo theoretical PDF-4, (b) Ni-L, (c) Co-L.

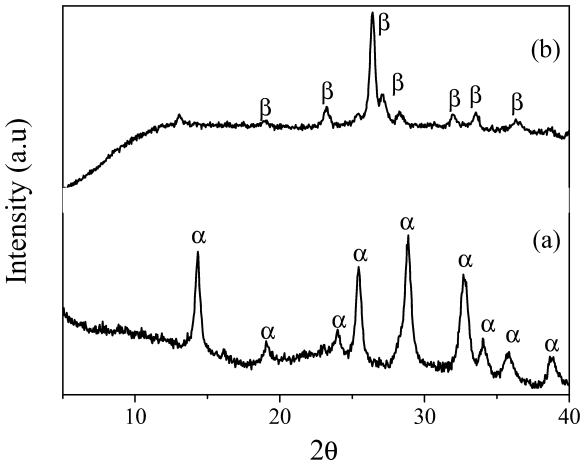

Fig. 2. XRD patterns of mixed oxides (a) Ni-O, (b) Co-O.

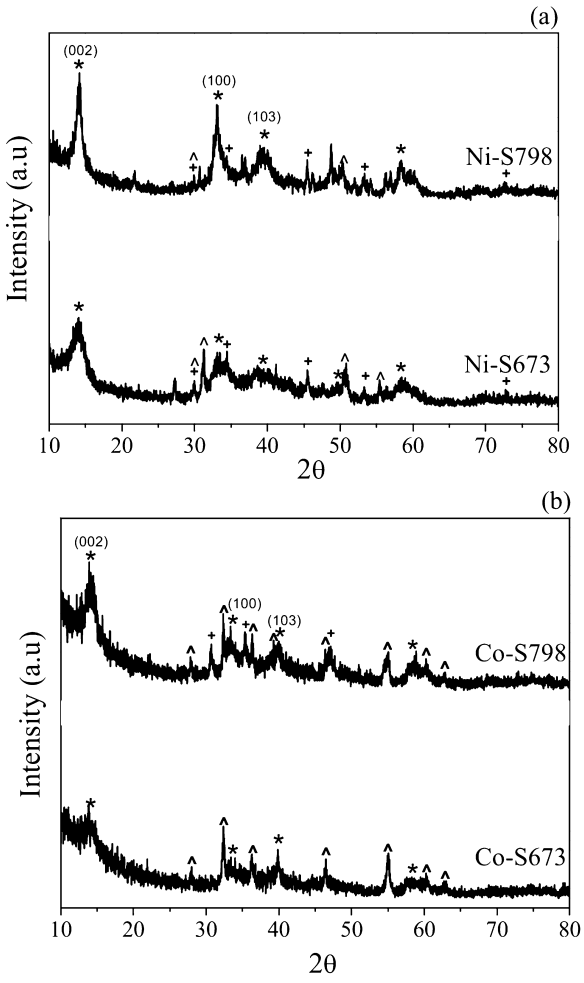

Fig. 3. XRD patterns of sulfide of (a) Ni-S673, Ni-S798 (b) Co-S673, Co-S798. *MoS_2 or *WS_2, $\hat{N}i_3S_2$ or $\hat{C}oS_2$, $^+$NiS or $^+$CoS.

Fig. 3 shows the XRD patterns for Ni-S673, Ni-S798 (Fig. 3a) and Co-S673, Co-S798 (Fig. 3b) obtained by *ex situ* activation. All the XRD patterns of the sulfided catalysts presented broad peaks due to the poor crystallinity of the materials. In both sulfided catalysts, molybdenum sulfide (MoS_2) and tungsten sulfide (WS_2) phases were identified from the PDF-4 database (codes 37-1492 and 8-0237, respectively) [20], although some characteristic signals of WS_2 match with MoS_2 at 14° (0 0 2), 33° (1 0 0), 39.5° (1 0 3), 50° (1 0 5) and 58° (1 1 0). Nickel sulfides (Ni_3S_2 and NiS) and cobalt sulfides (CoS_2 and CoS) were also observed in Fig. 3a and b, respectively; and were identified from the PDF-4 database (codes 44-1418, 65-5762 and 62-4856, 65-3418 respectively) [20].

The (0 0 2) corresponding reflection to MoS_2 and WS_2 was better defined in nickel-containing catalysts than in cobalt ones, which could indicate a higher stacking degree for Ni-SR673 and Ni-SR798 materials.

The stacking size of MoS_2 slabs determined by means of the Scherrer equation was in the range between 4.2 and 7.0 nm. From these results, it was evident that the promoters had an influence on the size of the nanocrystallites. By comparing the catalysts' patterns as a function of the activation temperature, an increase in crystallinity and intensity of the peaks were observed when the temperature was increased.

Table 2
Elemental analysis results of layer precursors and sulfided catalysts.

	wt%					
	Ni	Co	Mo	W	S	Ni(Co):Mo:W:S
Ni-L	25.3	–	25.5	19.3	–	1:0.6:0.2:0
Co-L	–	25.1	32.4	16.9	–	1:0.8:0.2:0
Ni-O	27.8	–	38.3	25.1	–	1:0.8:0.3:0
Co-O	–	29.7	38.8	16.5	–	1:0.8:0.2:0
Ni-SR673	34.5	–	30.9	12.1	22.5	1:0.5:0.1:1.1
Ni-SR798	36.9	–	29.2	11.7	22.2	1:0.5:0.1:1.1
Co-SR673	–	30.1	32.4	12.5	25.1	1:0.7:0.1:1.5
Co-SR798	–	28.0	34.3	10.2		

3.2. Elemental analysis

Chemical analysis by atomic absorption allowed quantifying the content of Mo, W and Ni or Co in the layered precursors this confirming that all materials are trimetallic. Table 2 reports the experimental percentages for Ni-L and Co-L materials. These results are in agreement with the chemical formula of Ni-L and Co-L compounds determined from the general formula proposed by Levin et al. [12] for the ϕ_y layer phase and with the results of thermal analysis, for $(NH_4)H_{1.4}Ni_{2.3}O(OH)(MoO_4)_{1.4}(WO_4)_{0.6}$ and $(NH_4)H_2Co_2O(OH)(MoO_4)_{1.6}(WO_4)_{0.4}$, respectively.

In Table 2, experimental percentages for Ni-O and Co-O materials are also reported. They are in agreement with the general formula proposed by Mazzocchia et al. [16] for α and β bimetallic phases for Ni-O and Co-O structures. These results are in accordance with the formulas proposed by Eqs. (4) and (5). Nickel and cobalt sulfides after reaction were analyzed by EDS (Table 2). These results confirm the presence of all the corresponding metals in the sulfide phase.

3.3. TGA and DSC analysis

TGA–DSC curves for the thermal decomposition of Ni-L and Co-L precursors are shown in Fig. 4a and b, respectively. The data obtained from the TGA–DSC studies of two catalysts precursors are summarized in Tables 3 and 4. DSC curves correspond to the decomposition of the catalysts precursors. In the two catalysts, few weight losses (2%) were observed around 370 K, with endothermic peaks that may be attributed to the elimination of impurities such as physisorbed water. In the case of the catalyst precursor Ni-L, two additional stages of weight losses are distinguishable; one of them about 5 wt% between 600 and 750 K is attributed to the elimination of H_2O as part of the molecular structure and the second one corresponds to a weight loss of 2 wt%, due to the elimination of NH_3 from 750 to 950 K. The elimination of H_2O and NH_3 is in agreement with the theoretical weight loss proposed as shown in reaction 4. In the case of Co-L precursor only one important step is shown from 400

Table 3
Summary of data obtained from the TGA–DSC studies for Ni-L.

Parameter	Ni-L
T_{-1} (K)	370
Δw_{-1}, wt% (experimental), assuming water (humidity)	2.0
Δw_1, wt% (experimental)	5.0
Δw_1, wt% (theoretical), assuming loss $1.7H_2O$	5.4
Δw_2, wt% (experimental)	2.0
Δw_2, wt% (theoretical), assuming loss NH_3	3.0
$\Sigma\Delta w$, wt% (experimental)	7.0
Residual, wt% (experimental)	91.0
Residual, wt% (theoretical), assuming residual as $NiMoO_4$, $NiWO_4$, NiO	91.6

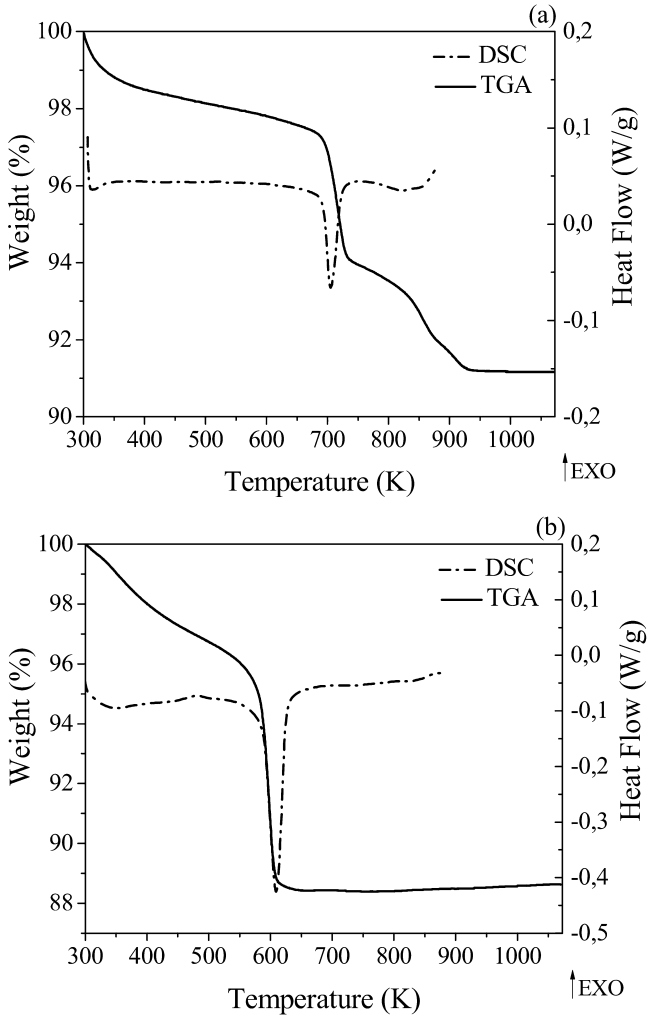

Fig. 4. TGA–DSC decomposition curves of (a) Ni-L, (b) Co-L.

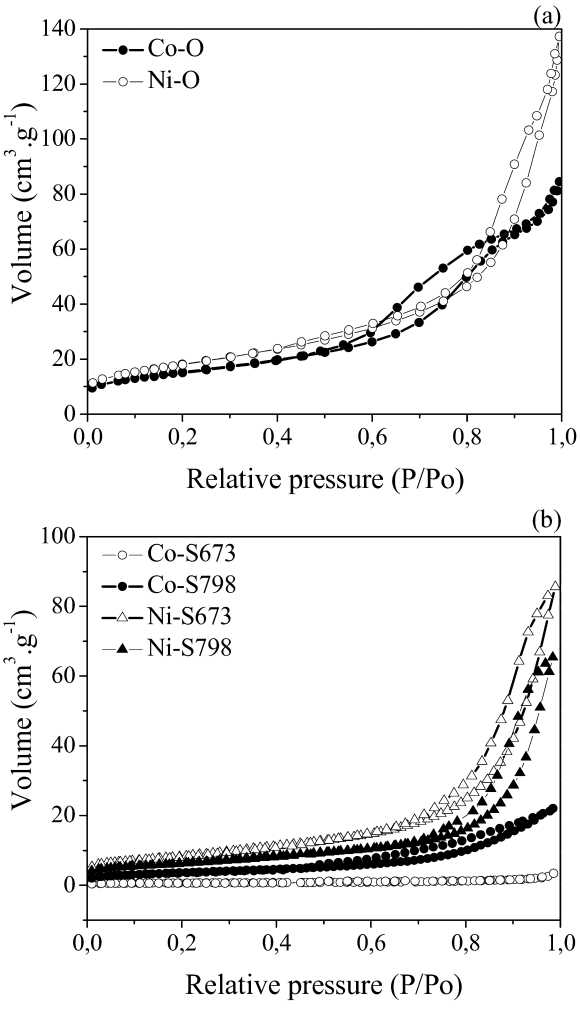

Fig. 5. Adsorption–desorption isotherms of (a) Ni-O and Co-O, (b) Ni-S673, Ni-S798, Co-S673 and Co-S798.

to 700 K attributed to the removal of NH_3 and H_2O simultaneously with a 10 wt% theoretical loss which is corroborated in reaction (5).

3.4. Textural properties

The N_2 adsorption–desorption isotherms of Ni-O and Co-O are presented in Fig. 5. It can be observed that the trimetallic mixed oxides show type IV isotherms, according to the Brunauer classification, an H2-type hysteresis for Co-O material, characteristic of inorganic solids with an intercommunicating porous net [25], and an H3-type hysteresis for the Ni-O material, corresponding to platelet aggregates [25].

Table 5 shows the surface areas and total pore volumes for the mixed oxides and sulfides. In this research, the layered phases obtained by co-precipitation and hydrothermal synthesis produced – after thermal decomposition – mesoporous mixed oxides with surface areas higher than those reported in other works using preparation methods such as freeze dried [17], sol–gel [18], and solid state [11].

The pore size distributions of Ni-O and Co-O mixed oxides are shown in Fig. 6. The Ni-O trimetallic oxide shows a wider pore size distribution, with two maxima at 4 nm and between 8 and 24 nm.

Table 4
Summary of data obtained from the TGA–DSC studies for Co-L.

Parameter	Co-L
T_{-1} (K)	370
Δw_{-1}, wt% (experimental), assuming water (humidity)	2.0
$T_1 - T_2$ (K)	400–700
Δw_2, wt% (experimental)	10.0
Δw_1, wt% (theoretical), assuming loss $NH_3 + 2H_2O$	10.0
Residual, wt% (experimental)	88
Residual, wt% (theoretical), assuming residual as $0.6CoMoO_4$, $0.4CoWO_4$	90

Table 5
Specific surface area and total pore volumes of the mixed oxides and sulfided materials.

Material	Surface area (m^2/g)	Total pore volume (cm^3/g)
Ni-O	65	0.21
Ni-S673	30	0.13
Ni-S798	23	0.10
Co-O	55	0.13
Co-S673	2	0.01
Co-S798	13	0.03

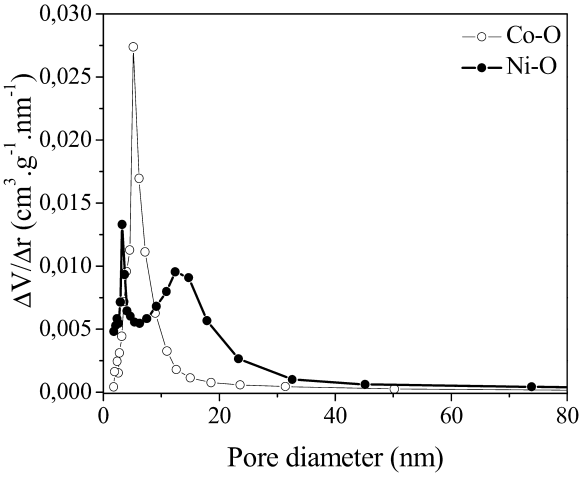

Fig. 6. Pore size distributions of the mixed oxides.

The Co-O only showed one peak around 5.2 nm, with a distribution range between 4.5 and 13 nm.

Mixed oxides treated with H_2S/H_2 at different temperatures allowed obtaining sulfided materials that are presented in Table 5. A high decrease in the surface areas and pore volumes were observed for all the catalysts. Nickel catalysts evidenced a decrease in the surface area and pore volume with an increase of the temperature. On the contrary, cobalt catalysts did not show this behavior. Co-S673 showed a surface area lower than Co-S798, that could be attributed to the small pore diameter (2.5 nm) compared with the other materials (greater than 5 nm). The formation of the CoS_2 phase, evidenced by XRD, is probably associated to pore blocking, causing difficulty for gas adsorption and diffusion through the material. Another reason to explain the low surface area of Co-S673 could be the uniformity of the material: the existence of both porous and no porous regions, the latter associated to CoS_2 phase. However, by increasing sulfurization temperature of Co-O at 798 K, the surface area was increased up to 6 times, which is attributed to a restructuring of unstable phase toward CoS, as observed in Fig. 3b. Nevertheless, the low surface area of the Co-S673 did not affect its catalytic activity, indicating that there is higher concentration of surface active sites compared to the Co-S798.

In Fig. 5b, N_2 adsorption–desorption isotherms of the sulfided catalysts are presented. The Ni-S673 and Ni-S798 presented type IV isotherms, characteristic of mesoporous materials, with an H3-type hysteresis [25]; however, cobalt sulfide catalysts did not evidence a real porosity due to their poor hysteresis loop; similar results were reported by others authors [9]. BJH pore size distribution (Fig. 7) supports the results of the isotherms, where nickel sulfide materials have pores with diameters between 5 and 35 nm, while the cobalt sulfide materials showed low concentrations of pores with diameter between 3 and 12 nm and peaks with small intensities.

3.5. H_2-TPR measurements

The H_2-TPR profiles are shown in Fig. 8. For Ni-O the reduction began at 573 K and two maximum peaks were observed at 751 and 1018 K. The shoulder observed near 800 K is probably due to the reduction of tungsten incorporated to the material. This behavior is typical of $NiMoO_4$ and $CoMoO_4$ bimetallic oxides [22,24], which is supported by the results obtained in XRD. For Co-O, two maximum peaks at 835 and 1080 K, and a shoulder near 885 K were also evidenced. In this case, the reduction initiated after 650 K could negatively influence the catalytic results. These results suggest that in the first reduction peak, a complete reduction of nickel or cobalt and partial reduction of Mo or W to the +3 oxidation states

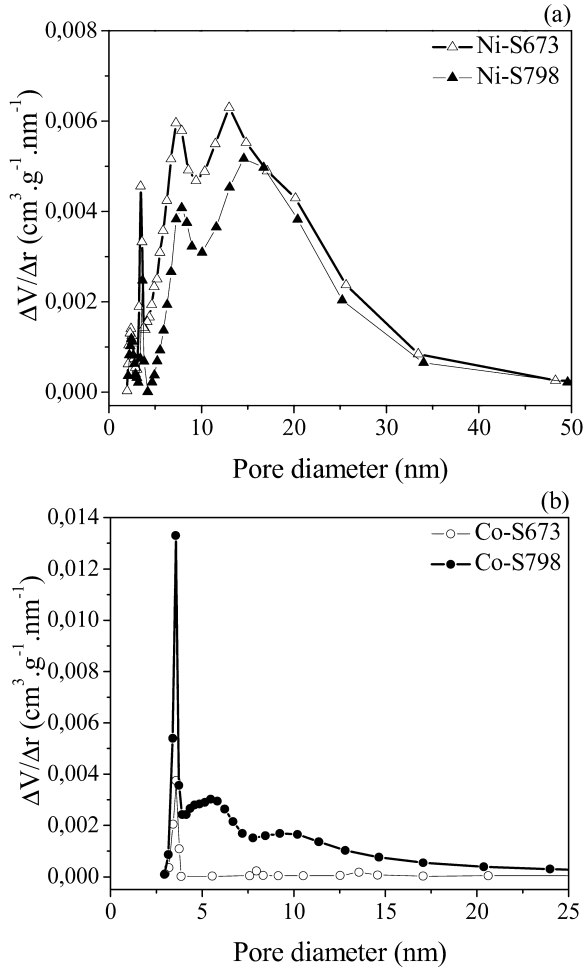

Fig. 7. Pore size distributions of sulfided materials (a) nickel, (b) cobalt.

are occurring [26]. In the second stage, reduction of molybdenum and tungsten is completed [26]. H_2-TPR profiles also showed shifts toward higher temperatures compared with $NiMoO_4$ and $CoMoO_4$ bimetallic oxides, which could be attributed to the low reducibility of tungsten.

The hydrogen uptake was calculated taking into account the general formula $Ni(Co)Mo_xW_{1-x}O_4$, where x was 0.26 and 0.20 for Ni-O and Co-O, respectively, determined by atomic absorption

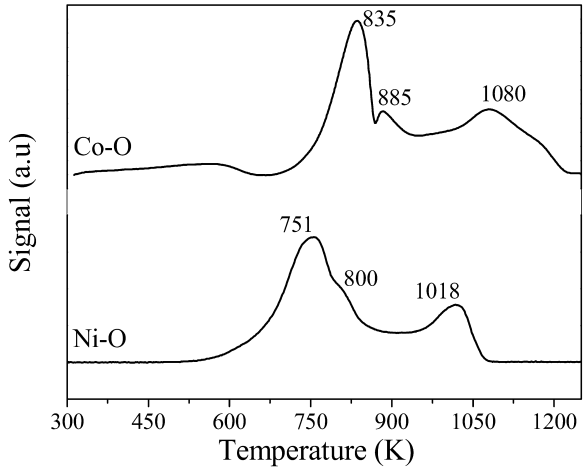

Fig. 8. H_2-TPR profiles of Ni-O and Co-O mixed oxides.

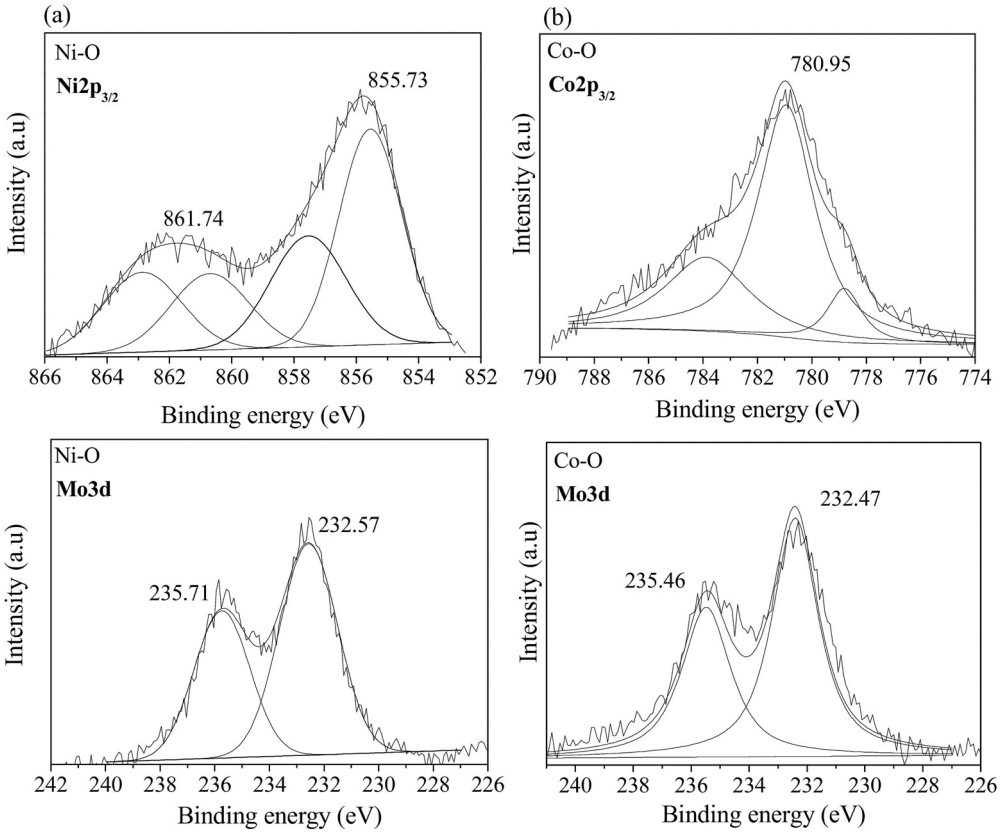

Fig. 9. High resolution XPS and deconvoluted signals of (a) Ni-O, (b) Co-O samples.

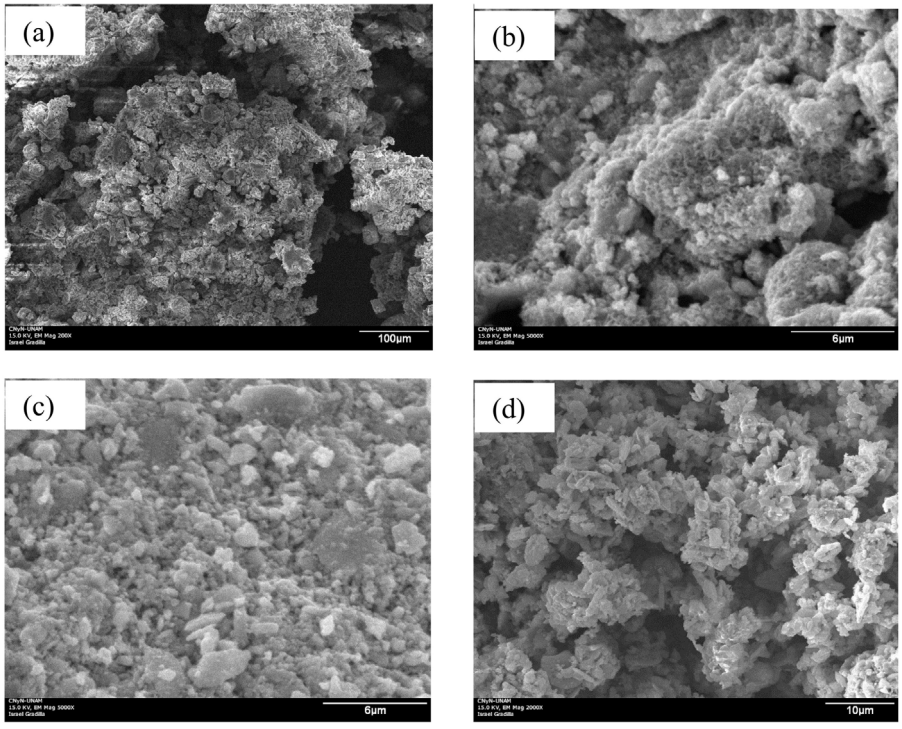

Fig. 10. Scanning electron micrographs of (a) Ni-SR673, (b) Ni-SR798, (c) Co-SR673, (d) Co-SR798.

spectrometry for tungsten. The calculated H_2 consumptions were 4.6 and 6.1 mol of hydrogen per mol of sample for Ni-O and Co-O, respectively. Ni-O showed the expected stoichiometry for complete reduction of the oxides; however, the Co-O required a higher amount of hydrogen for a complete reduction.

3.6. X-ray photoelectron spectroscopy (XPS)

In supplementary data Fig. S1, the survey scan of the Ni-O and Co-O mixed oxides are shown. In both oxides, peaks were observed around 35, 37, 232, 235 and 535 eV attributed to $W4f_{7/2}$, $W4f_{5/2}$, $Mo3d_{5/2}$, $Mo3d_{3/2}$, and O1s, respectively [27]. Signals corresponding to $Co2p_{3/2}$ and $Ni2p_{3/2}$ were found around 780 and 855 eV, respectively [27].

High resolution spectra of Ni-O and Co-O samples for regions corresponding to $Co2p_{3/2}$, $Ni2p_{3/2}$, $Mo3d_{5/2}$ and $Mo3d_{3/2}$ are presented in Fig. 9. Ni-O sample evidenced a main peak corresponding to the $Ni2p_{3/2}$ contribution with its corresponding satellites. $Ni2p_{3/2}$ main binding energy is observed at 855.5 eV. This result suggests that Ni^{+2} is present on the surface of the Ni-O oxide, according to previous reports [18,27–29]. For the Co-O sample, the main peak corresponding to the $Co2p_{3/2}$ contribution is observed at 780.9 eV with its respective satellites. The cobalt oxide species are attributed to Co^{+2}, which is in agreement with results obtained by other authors [30].

The Mo3d levels (Fig. 9a and b) of Ni-O and Co-O mixed oxides were also adjusted. The doublet pattern observed for molybdenum species is due to the spin-orbit splitting of Mo3d levels giving rise to $Mo3d_{5/2}$ and $Mo3d_{3/2}$ levels with binding energies around 232.5 and 235.7 eV, respectively for both materials. An energy separation of 3.1 eV and 3.0 eV for nickel and cobalt oxides respectively was measured [27,31]. From the above results, it could be inferred that the peak positions were consistent with MoO_3 [27,32] and it is confirmed that Mo is present mainly in the +6 oxidation state [27,31].

3.7. Scanning electron microscopy (SEM)

The morphologies of Ni-SR673, Ni-SR798, Co-SR673 and Co-SR798 catalysts after the HDS reaction were observed by SEM and are presented in Fig. 10. SEM images (Fig. 10a, c and d) showed disordered morphologies and different sizes, ranging from 2 to 4 μm. Ni-SR798 catalyst (Fig. 10b) presented a higher tendency to agglomerate than the Ni-SR673 one; therefore, the activation temperature had a great influence on the morphologies of the catalysts.

3.8. Transmission electron microscopy (TEM)

Fig. 11 reports the TEM images of nickel and cobalt catalysts after HDS reaction. All the catalysts presented homogeneity and typical structures of MoS_2 and WS_2 layers [3,33], and the fringes with an interlayer spacing between 0.616 and 0.647 nm and an average stacking number equal to 4 and 6 for cobalt- and nickel-containing catalysts, respectively. Average slab sizes also presented values between 5.5–6.7 nm for cobalt materials and 7.7–8.2 nm for nickel materials. These results are in agreement with previously published works [6,9].

Zhang et al. [6] showed in their work that the TEM images with stacking defects, mixed stacks and curvature planes are associated to a possible increase of active sites of the unsupported Ni-Mo-W sulfide catalyst. However, in this research, nickel-containing catalysts, a high proportion of fringes in TEM images are evidenced; moreover, the activation temperature and the promoter affected mainly the proportion of large slabs with curved morphology. Cobalt-containing catalysts showed a disorganized morphology; the slabs presented discontinuities due to the breaking of the layers, which suggested that the particles were less crystalline than nickel-containing catalysts. This is also supported by the XRD patterns (Fig. 3) where the cobalt materials presented a wide low intensity (0 0 2) diffraction peak [9,34].

3.9. Catalytic activity

The catalytic behavior for all catalysts is reported in Table 6. Cobalt and nickel materials were activated *ex situ* with a H_2/H_2S flow at two different temperatures: 673 and 798 K. Nickel catalysts exhibited higher activities than cobalt ones, at both activation temperatures, which could be associated to the curved morphology of nickel materials, because this could contribute to an increase of active sites in the sulfided catalyst [6,8,34]. This behavior could also be associated to the higher reduction capacity of the Ni-O towards the metallic state at low temperatures (Fig. 8), which allows a sulfidation easier than the Co-O. Contrary to nickel molybdates, the reduction of cobalt molybdates produced molybdate and spinel oxide phases [22] that could also be associated to their lower activity, due to the more difficult sulfidation of these stable oxides.

In XRD of sulfided materials (Fig. 3a and b), signals corresponding to α and β phases, which are inactive crystalline compounds for the HDS reaction [35] were not observed. Therefore, XRD results for the sulfided materials could indicate a successful sulfurization of the Ni-O and Co-O oxides. However, under the same sulfurization conditions, Ni-SR673 and Ni-SR798 materials showed differences with respect to the Co-SR673 and Co-SR798 catalysts, such as particle size, crystallinity, and intensity in the peaks, which could support the better activity in the HDS reaction of nickel containing catalysts.

Several authors [22,24] have suggested that the tetrahedral environment of Mo in the β-isomorphs provides better precursors for HDS reaction than α-isomorphs. This affirmation suggests that the Co-O oxide would have more interesting catalytic results that Ni-O; however, this behavior was not observed in this work. Ni-SR673 and Ni-SR798 solids obtained from α phase were more active in HDS reaction than in Co-SR673 and Co-SR798 catalysts obtained from β phase. In this case, it was not possible to compare α and β precursor oxides because the structures have different promoters (Ni and Co), and during the synthesis could not be obtained α and β phase for Ni-O and Co-O, but in fact they were obtained at lower temperatures and with higher surface area.

During the catalytic study, biphenyl (BP) and cyclohexylbenzene (CHB) were found. The first product (BP) was formed by the C—S bond cleavage of the DBT ring. This route is called direct desulfurization (DDS). The second product (CHB) was obtained by the hydrogenation of the aromatic ring and then, the C—S bond cleavage. This pathway is called hydrogenation (HYD) [2,36]. Both routes occur in parallel ways; however, each pathway depends on the nature of the sulfur compounds, the reaction conditions, catalysts, and promoters used [2]. In this work, the nickel catalysts had a much higher hydrogenation capacity than the cobalt catalysts, with HYD/DDS ratios equal to 1.9 and 3.4 for Ni-SR673 and Ni-SR798 respectively, compared to 0.2 for the two Co catalysts. This result could be attributed to the higher acidity and hydrogenation capacity of nickel with respect to cobalt [2,37].

Catalytic results were also compared with a commercial catalyst ($NiMo/\gamma\text{-}Al_2O_3$) [38] evaluated under the same reaction conditions. HYD/DDS ratios of Ni-SR673 and Ni-SR798 catalysts, achieved a DBT conversion of 20% (Table 6). These showed a higher selectivity toward HYD compared with the optimized commercial $NiMo/\gamma\text{-}Al_2O_3$ catalyst with a value equal to 0.5 [38]. However, commercial $NiMo/\gamma\text{-}Al_2O_3$ presented a higher activity (12×10^{-7} mol/s g) than Ni-SR673 (2.0×10^{-7} mol/s g) and Ni-SR798 (3.0×10^{-7} mol/s g).

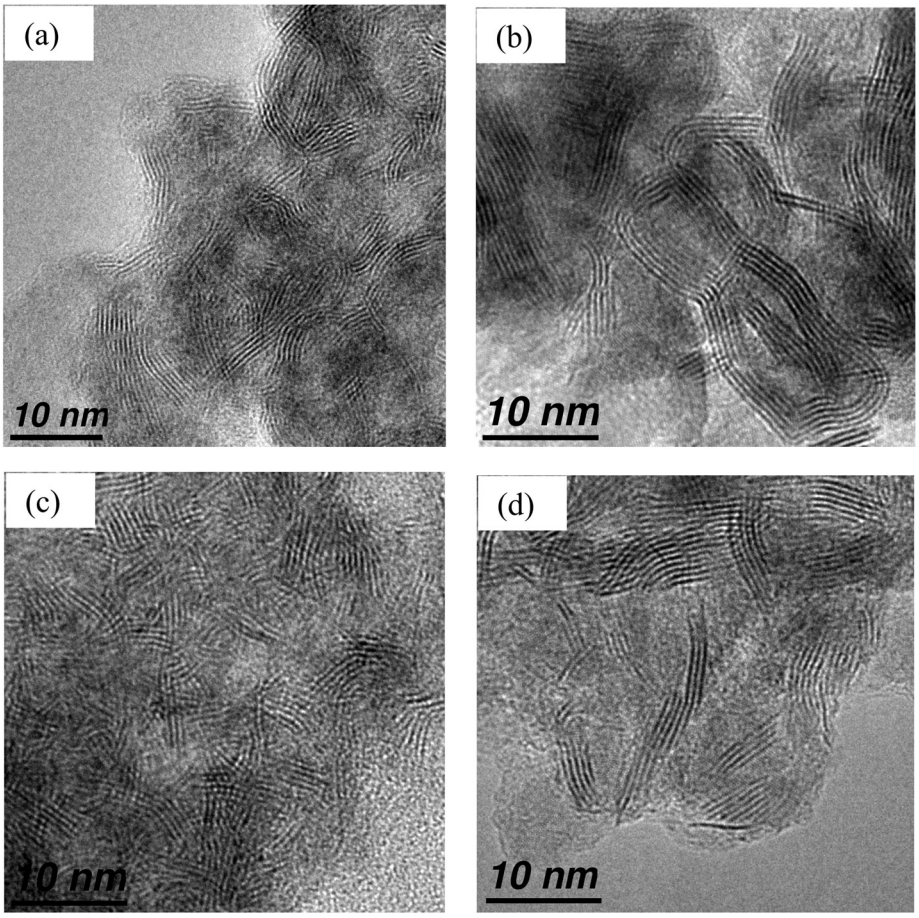

Fig. 11. Transmission electron micrographs of (a) Ni-SR673, (b) Ni-SR798, (c) Co-SR673, (d) Co-SR798.

Table 6
Effect of the promoter and activation temperature in the activity of the trimetallic catalysts in HDS of DBT.

Catalysts	DBT conversion (%)	HYD/DDS[a]	Selectivity (%)		Initial reaction rate ($\times 10^{-8}$ mol/s g)
			CHB	BP	
Co-SR673	25	0.2 (0.2)	18	82	8.5
Co-SR798	14	0.2 (0.1)	14	86	4.8
Ni-SR673	68	1.9 (0.9)	65	35	19.5
Ni-SR798	93	3.4 (1.3)	77	23	30.2

[a] HYD/DDS = (CHB + THDBT)/(BP). Values inside the parentheses are HYD/DDS ratios achieved at a DBT conversion of 20%.

The last ones were in the same order of magnitude of some unoptimized NiMo sulfides supported on SBA-15 [38]. According with previous studies [3,38], the type of precursors, synthesis conditions, and molar compositions are fundamental for the production and optimization of active materials for the HDS reaction. Therefore, future studies could be focused toward the modification of molar relations for the system with Ni-Mo-W, using less amount of nickel in the synthesis, due to the possible formation of nickel-sulfides phases that could cover the surface of active sites of the catalyst [38].

In this research, Ni-SR798 catalyst showed a higher DBT conversion (equal to 93%) followed by Ni-SR673 (equal to 68%) where both values were obtained after 5 h of reaction. Therefore, these results confirm previous results obtained in another research [39], that is, the overall activity of these unsupported catalysts is being mainly determined by the nature of the divalent metal rather than by the nature of the group 6 metal. It has been shown before that unsupported NiMo and NiW sulfides were considerably more active in the HDT of the same model feed than CoMo and CoW sulfides [39].

4. Conclusions

Thermal decomposition of Ni-L and Co-L layered precursors allowed obtaining α and β mixed oxides, respectively, at temperatures as low as 673 K, mesoporous, and with surface areas above 50 m^2/g. This last property is higher than those reported in the open literature. Divalent metal and activation temperature influenced the structural, textural, and morphological properties of the sulfided catalysts which were evidenced in the results of characterization and catalysis. Nickel catalysts exhibited higher activities than the cobalt ones in the HDS reaction with DBT – the molecule under study – which could be associated to the tetrahedral or octahedral coordination of the hexavalent metal in the precursor mixed oxide, to the activation temperature up to 798 K, and it could also be explained by the higher hydrogenation capacity observed by H_2-TPR, and the defects of mixed stacking and curves observed in TEM that could contribute to an increase of active sites. The results obtained in this research are of great scientific

value. They could be improved if the molar relations for the system with Ni-Mo-W are modified using less amount of nickel in the synthesis.

Acknowledgements

We acknowledge financial support of the Universidad de Antioquia and 2013–2014 Sustainability Program. We also acknowledge Centro de Nanociencias y Nanotecnología, Universidad Nacional Autónoma de México and the valuable technical assistance of J.A. Díaz, I. Gradilla, M. Curiel, J.N. Díaz de León, F. Ruiz, J. Mendoza and E. Aparicio, as well as, to Dr. Arnaldo Faro, Universidade Federal de Río de Janeiro, Río de Janeiro, Brasil, for collecting the surface area data for mixed oxides samples. S. Amaya acknowledges COLCIENCIAS her doctoral fellowship.

Appendix A. Supplementary data

Supplementary material related to this article can be found, in the online version, at http://dx.doi.org/10.1016/j.apcatb.2013.10.057.

References

[1] A. Stanislaus, A. Marafi, M.S. Rana, Catal. Today 153 (2010) 1–68.
[2] I.V. Babich, J.A. Moulijn, Fuel 82 (2003) 607–631.
[3] H. Topsøe, B.S. Clausen, F.E. Massoth, in: J.R. Anderson, M. Boudart (Eds.), Hydrotreating Catalysis—Science and Technology, vol. 11, Springer-Verlag, Berlin, 1996, pp. 1–269.
[4] C. Song, Catal. Today 86 (2003) 211–263.
[5] R.R. Chianelli, G. Berhault, P. Raybaud, S. Kasztelan, J. Hafner, H. Toulhoat, Appl. Catal. A: Gen. 227 (2002) 83–96.
[6] B.S. Zhang, Y.J. Yi, W. Zhang, C.H. Liang, D.S. Su, Mater. Charact. 62 (7) (2011) 684–690.
[7] S. Mignard, S. Kaztelan, M. Dorbon, A. Billon, P. Sarrazin, Stud. Surf. Sci. Catal. 100 (1996) 209–216.
[8] S. Eijsbouts, S.W. Mayo, K. Fujita, Appl. Catal. A: Gen. 322 (2007) 58–66.
[9] R. Romero-Rivera, G. Berhault, G. Alonso-Núñez, M. del Valle, F. Paraguay-Delgado, S. Fuentes, S. Salazar, A. Aguilar, J. Cruz-Reyes, Appl. Catal. A: Gen. 433–434 (2012) 115–121.
[10] J. Bocarando, R. Huirache-Acuña, W. Bensch, Z.D. Huang, V. Petranovskii, S. Fuentes, G. Alonso-Núñez, Appl. Catal. A: Gen. 363 (2009) 45–51.
[11] J.M. Quintana-Melgoza, J. Cruz-Reyes, M. Avalos-Borja, Mater. Lett. 47 (2001) 314–318.
[12] D. Levin, S.L. Soled, J.Y. Ying, Inorg. Chem. 35 (1996) 4191–4197.
[13] L. Palacio, A. Echavarría, C. Saldarriaga, Int. J. Inorg. Mater. 3 (2001) 367–371.
[14] H. Pezerat, Bull. Soc. Fr. Minéral. Cristallogr. 90 (1967) 549–557.
[15] H. Rase, Handbook of Commercial Catalysts, CRC Press, New York, 2000.
[16] C. Mazzocchia, A. Kaddouri, R. Anouchinsky, M. Sautel, G. Thomas, Solid State Ionics 63–65 (1993) 731–735.
[17] D. Vie, E. Martínez, F. Sapiña, J.-V. Folgado, A. Beltrán, Chem. Mater. 16 (2004) 1697–1703.
[18] A. Kaddouri, E. Tempesti, C. Mazzocchia, Mater. Res. Bull. 39 (2004) 695–706.
[19] T.K. Ghorai, D. Dhak, S. Dalai, P. Pramanik, J. Alloys Compd. 463 (2008) 390–397.
[20] International Centre for Diffraction Data ICDD, Powder Diffraction File PDF-4, 2009.
[21] A. Guinier, X-Ray Diffraction in Crystals, Imperfect Crystals, and Amorphous Bodies, Dover Publications, New York, 1994.
[22] J. Brito, L. Barbosa, J. Catal. 171 (1997) 467–475.
[23] J.L. Brito, J. Thermal Anal. 49 (1997) 535–540.
[24] J. Brito, A. Barbosa, A. Albornoz, F. Severino, J. Laine, Catal. Lett. 26 (1994) 329–337.
[25] K.S.W. Sing, D.H. Everett, R.A.W. Haul, L. Moscou, R.A. Perotti, J. Rouquérol, T. Siemieniewska, Pure Appl. Chem. 57 (4) (1985) 603–619.
[26] M. Salamanca, Y.E. Licea, A. Echavarría, A. Faro, L.A. Palacio, Phys. Chem. Chem. Phys. 11 (2009) 9583–9591.
[27] J.F. Moulder, W.F. Stickle, P.E. Sobol, K.D. Bomben, Handbook of X-ray Photoelectron Spectroscopy, PerkinElmer Corporation, Minessota, 1992.
[28] R.M. Martin-Aranda, M.F. Portela, L.M. Madeira, F. Freire, M. Oliveira, Appl. Catal. A: Gen. 127 (1995) 201–217.
[29] A.P. Grosvenor, M.C. Biesinger, R.St.C. Smart, N.S. McIntyre, Surf. Sci. 600 (2006) 1771–1779.
[30] A.D. Gandubert, C. Legens, D. Guillaume, S. Rebours, E. Payen, Oil Gas Sci. Technol. 62 (1) (2007) 79–93.
[31] G.E. Buono-Core, G. Cabello, A.H. Klahn, A. Lucero, M.V. Núñez, B. Torrejón, C. Castillo, Polyhedron 29 (2010) 1551–1554.
[32] E.I. Altman, T. Droubay, S.A. Chambers, Thin Solid Films 414 (2002) 205–215.
[33] Y. Gochy, C. Ornelas, F. Paraguay, S. Fuentes, L. Álvarez, J.L. Rico, G. Alonso-Núñez, Catal. Today 107–108 (2005) 531–536.
[34] A. Nogueira, R. Znaiguia, D. Uzio, P. Afanasiev, G. Berhault, Appl. Catal. A: Gen. 429–430 (2012) 92–105.
[35] S. Eijsbouts, in: K.P. de Jong (Ed.), Synthesis of Solid Catalysts, Wiley-VCH, Weinheim, 2009, pp. 301–328.
[36] M.J. Girgis, B.C. Gates, Ind. Eng. Chem. Res. 30 (1991) 2021–2058.
[37] J. Vila, F. Sapiña, E. Martínez, V. Cortés, J. Podobinski, Contrib. Sci. 4 (2) (2008) 223–229.
[38] Z.-D. Huang, W. Bensch, L. Kienle, S. Fuentes, G. Alonso, C. Ornelas, Catal. Lett. 127 (2009) 132–142.
[39] S.L. Amaya, Y.E. Licea, M. Salamanca, A. Faro, A. Echavarría, L.A. Palacio, Rev. Fac. Ing. Univ. Antioquia (56) (2010) 58–67.